Received: 23 November 2019 | Revised: 8 April 2020 | Accepted: 12 April 2020

DOI: 10.1002/eqe.3283

WILEY

RESEARCH ARTICLE

Dynamics and seismic performance of rocking bridges accounting for the abutment-backfill contribution

Ioannis M. Thomaidis[1] | **Andreas J. Kappos**[2] | **Alfredo Camara**[1]

[1]Department of Civil Engineering, City, University of London, London, UK

[2]Department of Civil Infrastructure and Environmental Engineering, Khalifa University, Abu Dhabi, United Arab Emirates

Correspondence
Ioannis M. Thomaidis, Department of Civil Engineering, City, University of London, London, UK.
Email: ioannis.thomaidis@city.ac.uk

Summary

The present study explores analytically the concept of rocking isolation in bridges considering for the first time the influence of the abutment-backfill system. The dynamic response of rocking bridges with free-standing piers of same height and same section is examined assuming negligible deformation for the substructure and the superstructure. New relationships for the prediction of the bridge rocking motion are derived, including the equation of motion and the restitution coefficient at each impact at the rocking interfaces. The bridge structure is found to be susceptible to a failure mode related to the failure of the abutment-backfill system, which can occur prior to the well-known overturning of the rocking piers. Thus, a new failure spectrum is proposed called Failure Minimum Acceleration Spectrum (FMAS) which extends the overturning spectrum put forward in previous studies, and it differs in principle from the latter. The comparison with the dynamic response of bridges modelled as rocking frames without abutments reveals not only that seat-type abutments and their backfill have a generally beneficial effect on the seismic performance of rocking pier bridges by suppressing the free rocking motion of the frame system, but also that the simple frame model cannot capture all salient features of the rocking bridge response as it misses potential failure modes, overestimating the rocking bridge's safety when these modes are critical.

KEYWORDS

abutment, analytical dynamics, backfill, rocking bridges, seismic isolation, self-centring

1 | INTRODUCTION

Development of transport networks currently faces the challenge of reducing construction time as well as damage and downtime costs when strong earthquakes or other extreme natural hazards occur. Bridges designed according to modern standards have a generally satisfactory behaviour in terms of collapse prevention during strong seismic events, however, they also suffer significant damage (bridges with ductile piers) and/or permanent displacements (bridges with ductile piers or "conventional" seismic isolation if not provided with adequate recentring capability). These problems resulted in the past in significant disruptions of the operation of transport networks and incurred significant

economical and societal losses. In this context, structural rocking (also called pier rocking) has emerged as a promising isolation technique for bridges.[1] Structural systems that utilise rocking as an isolation technique display minimal damage,[2] inherent recentring capacity[3] and negative stiffness that avoids resonance.[4] Moreover, rocking can be particularly relevant in Accelerated Bridge Construction (ABC) which has been gaining substantial momentum worldwide due to the important advantages that it offers over the conventional construction methods, namely, construction efficiency and potentially lower costs. The adequacy of rocking systems in seismic situations depends strongly on the behaviour of rocking interfaces (at the top, bottom and throughout the length of the piers) (previous studies[5–7] among others) as well as the possible lack of recentring of the supporting members, especially when the vertical component of the ground motion is significant.[8] The latter is usually mitigated with unbonded posttensioned tendons (previous studies[5,9,10] among others). So far, there is a very small number of rocking bridges constructed in regions with moderate or high seismicity. Two examples are the South Rangitikei Bridge,[11,12] which has shown remarkable seismic performance after several strong ground motions,[13] and the Wigram-Magdala Link Bridge,[14] both located in New Zealand.

Housner[15] paved the way for modern analytical studies on rocking, which set the basis for implementation of this type of isolation in structural systems that could be of interest for bridges. The systems studied were single columns (Zhang and Makris and DeJong and Dimitrakopoulos[16,17] among others) and frames (Makris and Vassiliou and Dimitrakopoulos and Giouvanidis[18,19] among others) and the results showed a remarkable stability of these systems against strong earthquakes. However, the rocking frame used in these analytical works neglects the influence of the abutment-backfill system which is not included in the formulation, even in studies that aim to address the rocking movement of bridges. Seat-type abutments and embankments are often considered as earth-retaining systems designed to provide only traffic access to and from the bridge. However, it has been found that the abutment typology and the stiffness of the backfill/embankment can influence significantly the global response of bridges subject to moderate to strong ground motions.[20] This is mainly due to the reduction of displacement demand in the piers.[21] Several studies addressed aspects of the abutment-backfill system such as the nonlinear behaviour of its components and the formation of a gap between the abutment and the backfill (previous studies[22–24] among others); however, the abutments are not expected to fail under seismic actions in conventional bridge typologies.[25] Recent studies like[24] have also addressed the important issue of the uncertainties involved in the modelling of the abutment-backfill system. Pier failure was also the focus in numerical studies where bridges with rocking piers were examined,[26] assuming that the structure fails only when overturning of the piers occurs due to excessive horizontal displacement. However, the case that the abutment-backfill fails prior to pier overturning was not considered; hence, ignoring that a different collapse hierarchy can be found in bridges that develop significant pier drifts, as in rocking structures,[27] potentially rendering the abutments the most vulnerable component of the bridge system.[28]

In the light of the previous remarks, the present study examines the two-dimensional seismic response of straight rocking bridges with free-standing piers of equal height and same rectangular section (i.e., symmetric bridges). The Equation of Motion (EoM) is formulated accounting for the abutment-backfill effect in the rocking response. This is modelled using the common simplification of an equivalent linear spring and a linear dashpot element working in parallel in the longitudinal (along-drive) direction, while in the vertical direction the abutment supports the deck, reducing the part of its weight that goes to the piers. The effect of vertical support by the abutments is included in a new expression for the restitution coefficient that is derived using an impulse formulation. A new failure criterion is integrated in the assessment of rocking of bridges to predict the collapse of the abutments due to large longitudinal displacement induced by the deck. This leads to the development of a new type of failure spectrum that extends the existing Overturning Minimum Acceleration Spectrum (OMAS). The effect of the abutment-backfill system in the rocking seismic response is established by comparing the seismic performance of rocking bridges with that of equivalent rocking frames without abutments.

2 | ANALYTICAL MODEL OF THE ROCKING RESPONSE OF SYMMETRIC BRIDGES

This section includes the effect of the abutment-backfill system that is characteristic of bridge structures in the formulation of the planar longitudinal rocking response of symmetric frames.[18] Figure 1 illustrates a symmetric bridge subjected to a horizontal ground acceleration history $\ddot{u}_g$. The generic bridge has N piers and a total length $L_{tot} = 2L_1+(N-1)L_2$, where L_1 and L_2 denote the length of the end and the intermediate spans, respectively. It is assumed that the superstructure consists of a continuous box girder section with depth $2h$, whereas the piers have a

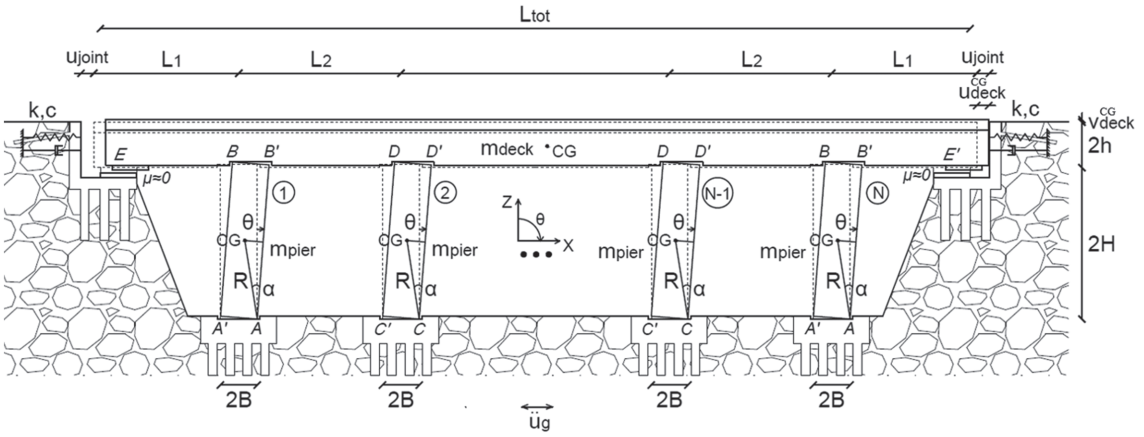

FIGURE 1 Schematic of a symmetric rocking bridge with ***N*** rectangular free-standing piers, and the model of the abutment-backfill system

height of 2*H* and rectangular cross-sections with a dimension of 2*B*. Special grooved caps are introduced at both pier ends to confine the rocking motion within the two horizontal planes of the bridge, thus ignoring three-dimensional rocking response[29]; addressing the rocking response in the transverse direction is beyond the scope of this paper. The deformability of all structural members is ignored without a significant loss of accuracy,[26] but with gains in simplicity and computational efficiency. The piers are designed to rock freely on the foundation (pivots A′-A and C′-C) and the deck (pivots B-B′ and D-D′) interfaces, without sliding at any instant.[30,31] From a construction perspective, this can be achieved by means of grooves provided on the top surface of the foundation and on the soffit of the deck, although a small level of sliding could occur in reality, especially for slender blocks.[32] Low-friction ($\mu \approx 0$) sliding concave steel bearings are introduced at each abutment seat (points E and E′, as shown in Figure 1) providing negligible constraint to the movement of the deck in the longitudinal direction while they can follow the up-and-down (cyclic vertical) motion of the superstructure. The combined effect of the seat-type abutment and the backfill in the longitudinal direction is represented by a spring (k) and a dashpot (c) element at each end of the deck, whereas in the vertical direction supports (E and E′) are introduced to represent the abutment seats. These longitudinal elements are activated when the deck closes the end joint gap (u_{joint}) whereas the vertical supports E and E′ are engaged when the bridge system returns to the at-rest position.

2.1 | Kinematics

Figure 1 shows the bridge experiencing longitudinal and vertical motions induced by the rocking motion of the free-standing piers around the corresponding pivot points at their bases (A and C). Due to the symmetry of the system, all piers undergo identical movement and, therefore, the superstructure experiences a purely translational motion (longitudinal, along-X and vertical, along-Z) that is driven by the pivot points located at the top of the piers (B and D), without relative rotations about the transverse (Y) axis.[19] Consequently, the dynamic motion of this bridge configuration can be captured with a single Degree of Freedom (DOF), which is selected to be the relative rotation of each pier with respect to the at-rest position (θ).

The key parameters that influence the dynamics of the rocking bridge are the total mass of the structure, the mass moment of inertia of the rectangular rocking piers with respect to their Centre of Gravity (CG) ($I_{pier}^{CG} = m_{pier}R^2/3$) and the dimensions of the piers. The total mass of the structure is composed of the mass of the superstructure (m_{deck}) and the substructure (Nm_{pier}). This mass constitutes an inherent restoring mechanism for the rocking system so long as the piers have not passed the overturning threshold. The effect of the pier dimensions on the rocking motion is described by means of their diagonal length ($R = \sqrt{H^2 + B^2}$) and their slenderness ($\alpha = \tan^{-1}(B/H)$). When the bridge structure undergoes rocking motion without toppling, the longitudinal u (X) and vertical v (Z) relative displacements of the CG of the piers and the deck with respect to the pertinent point at the at-rest position of each member are expressed in terms of the independent variable θ according to Equations 1 to 4, respectively

$$u_{pier}^{CG} = \mathrm{sgn}(\theta)R[\sin a - \sin(a - |\theta|)], \tag{1}$$

$$v_{pier}^{CG} = R[\cos(a - |\theta|) - \cos a], \tag{2}$$

$$u_{deck}^{CG} = \mathrm{sgn}(\theta)2R[\sin a - \sin(a - |\theta|)], \tag{3}$$

$$v_{deck}^{CG} = 2R[\cos(a - |\theta|) - \cos a], \tag{4}$$

where $\mathrm{sgn}(\theta)$ is the sign function of θ. The convention for positive rotations and displacements is shown in Figure 1.

2.2 | Rocking initiation

The rocking motion of the bridge structure initiates when the lateral ground motion reaches a minimum acceleration ($\ddot{u}_{g,\min}$) that is capable of inducing uplift in the entire system. Considering that the sliding bearings at the abutments do not restrain the longitudinal motion of the superstructure, application of the principle of virtual work when the bridge starts rocking gives

$$m_{deck}\ddot{u}_{g,\min}\delta u_{deck}^{CG} + Nm_{pier}\ddot{u}_{g,\min}\delta u_{pier}^{CG} = m_{deck}g\delta v_{deck}^{CG} + Nm_{pier}g\delta v_{pier}^{CG}, \tag{5}$$

where g is the gravitational acceleration and

$$\delta {u_i}^{CG} = \frac{\partial {u_i}^{CG}}{\partial \theta}\delta\theta \text{ and } \delta {v_i}^{CG} = \frac{\partial {v_i}^{CG}}{\partial \theta}\delta\theta, \tag{6}$$

where i refers to the deck and pier members, respectively. Taking into account that the rocking motion has just started at this instant (i.e., $\theta = 0$), and introducing Equations 6 and 1 to 4 into Equation 5, the minimum ground acceleration that is required to initiate the rocking motion is

$$m_{deck}\ddot{u}_{g,\min}(2R\cos a) + Nm_{pier}\ddot{u}_{g,\min}(R\cos a) = \mp m_{deck}g(2R\sin a) \mp Nm_{pier}g(R\sin a). \tag{7}$$

Simplifying Equation 7 yields the minimum acceleration needed to uplift the bridge structure

$$\ddot{u}_{g,\min} = \mp \lambda g \tan a, \tag{8}$$

where $\lambda = 1$ for a symmetric rocking bridge. The double sign formulation ($\mp$) in Equations 7 and 8 denotes that the bridge will initially rock with a positive (clockwise) rotation only if the horizontal ground acceleration has a negative value (i.e., the ground is accelerating to the left in Figure 1) and vice-versa. According to Equation 8, the minimum acceleration that initiates rocking motion of the bridge structure depends only on the slenderness of the piers (α), while it is independent of the direction of the movement, the mass of the deck (m_{deck}) and the properties of the abutment-backfill system. It is noted that this result is the same as that in the corresponding rocking frame, wherein the effect of the abutments and the backfill is ignored.[18] This is because their influence on the rocking motion starts only after rocking is initiated, that is, when the joint gap (u_{joint}) is closed and the deck impacts longitudinally on one abutment backwall, or when the deck returns to its original position and impacts on the abutment seats.

2.3 | EoM during rocking

Considering that the ground motion is strong enough to initiate rocking of the bridge in Figure 1 (i.e., $\max(|\ddot{u}_g|) > |\ddot{u}_{g,\min}|$), its response can be described by the energy balance using Lagrange equation

$$\frac{d}{dt}\left(\frac{\partial T}{\partial \dot{\theta}}\right)-\frac{\partial T}{\partial \theta}+\frac{\partial V}{\partial \theta}=Q, \tag{9}$$

where T is the kinetic energy of the rocking system, V is the potential energy produced by the conservative forces and Q expresses the effect of the nonconservative forces. The generalised coordinate that describes the rocking motion is the rotation θ, and its first time-derivative $\dot{\theta}$ describes the angular velocity of the rocking piers. The kinetic energy of the system with respect to the corresponding CG of the members can be expressed as

$$T=N\frac{1}{2}I_{pier}^{CG}\dot{\theta}^2+N\frac{1}{2}m_{pier}\left(\dot{u}_{pier}^{CG\ 2}+\dot{v}_{pier}^{CG\ 2}\right)+\frac{1}{2}m_{deck}\left(\dot{u}_{deck}^{CG\ 2}+\dot{v}_{deck}^{CG\ 2}\right), \tag{10}$$

where $\dot{u}_{pier}^{CG}$, $\dot{v}_{pier}^{CG}$, $\dot{u}_{deck}^{CG}$, $\dot{v}_{deck}^{CG}$ are the longitudinal and vertical velocities of the CG of the piers and the deck, respectively. These are obtained as the first time-derivatives of Equations 1 to 4. Simplifying Equation 10 yields

$$T=\left[\frac{N}{2}I_{pier}^{Pivot}+2m_{deck}R^2\right]\dot{\theta}^2, \tag{11}$$

wherein $I_{pier}^{Pivot}=4m_{pier}R^2/3$ is the mass moment of inertia of the rocking pier with respect to the pertinent pivot point (A and C for positive-clockwise rotation or A′ and C′ for negative-counterclockwise rotation). The total potential energy in the rocking bridge (V) is introduced by the gravitational effects (V_{in}) and by the elastic spring forces of the abutments (V_{as}), $V=V_{in}+V_{as}$. The term V_{in} expresses the total weight of the system which tends to return the rocking bridge to its equilibrium position, and it is given by

$$V_{in}=\mathrm{g}\left(Nm_{pier}v_{pier}^{CG}+m_{deck}v_{deck}^{CG}\right), \tag{12}$$

where v_{pier}^{CG} and v_{deck}^{CG} are given by Equations 2 and 4, respectively. The term V_{as} expresses the longitudinal constraint of the abutment-backfill system to the free rocking motion of the structure, and it is active only when the deck is in contact with the abutments by closing the joint gap

$$V_{as}=\left\{\begin{array}{c}0\\ \frac{1}{2}k\left(u_{deck}^{CG}-\mathrm{sgn}(\theta)u_{joint}\right)^2\end{array}\right\}\ \text{if}\quad\left\{\begin{array}{l}\left|u_{deck}^{CG}\right|<u_{joint}\\ \left|u_{deck}^{CG}\right|\geq u_{joint}\end{array}\right\}. \tag{13}$$

Substituting Equations 2 to 4 into Equations 12 and 13 gives the total effect of the conservative forces on the rocking system

$$V=\left\{\begin{array}{l}\mathrm{g}R\left[Nm_{pier}+2m_{deck}\right]\left(\cos(\alpha-|\theta|)-\cos a\right)+2kR^2\\ \left[\begin{array}{l}\sin^2 a-2\sin a\sin(\alpha-|\theta|)+\sin^2(\alpha-|\theta|)\\ -\sin a\frac{u_{joint}}{R}+\sin(\alpha-|\theta|)\frac{u_{joint}}{R}+\frac{u_{joint}^2}{4R^2}\end{array}\right]\end{array}\right\}. \tag{14}$$

Equation 14 is presented in its complete form accounting for the longitudinal contact of the deck with the abutments. Prior to contact (i.e., $\left|u_{deck}^{CG}\right|<u_{joint}$), the term containing the spring stiffness (k) is excluded from calculation. The variation of the virtual work δW_{nc} describes the effect of the generalised nonconservative forces required for the Lagrangian Equation 9

$$\delta W_{nc}=Q\delta\theta\Rightarrow\delta W_{in}+\delta W_{ad}=(Q_{in}+Q_{ad})\delta\theta, \tag{15}$$

where $\delta W_{in}=-\ddot{u}_g\left(Nm_{pier}u_{pier}^{CG}+m_{deck}u_{deck}^{CG}\right)$ represents the external work introduced in the system by the ground acceleration, $\delta W_{ad}=-c\,\dot{u}_{deck}^{CG}\left(u_{deck}^{CG}-\mathrm{sgn}(\theta)u_{joint}\right)$ is the energy dissipated by the interaction between the deck and the

backfill through the dashpot elements used to model it and u_{pier}^{CG} and u_{deck}^{CG} are given by Equations 1 and 3, respectively. The corresponding generalised forces $Q_{in} = \partial W_{in}/\partial\theta$ and $Q_{ad} = \partial W_{ad}/\partial\theta$ are given by

$$Q_{in} = -\ddot{u}_g R\left(Nm_{pier} + 2m_{deck}\right)\cos(\alpha - |\theta|), \tag{16}$$

$$Q_{ad} = -4cR^2\cos^2(\alpha - |\theta|)\dot{\theta}. \tag{17}$$

Introducing Equations 11, 14, 16, 17 into Equation 9 yields the equation of rocking motion for the symmetric bridge structure

$$\ddot{\theta} = \overbrace{-p^2\frac{1+2\gamma}{1+3\gamma}\left[\operatorname{sgn}(\theta)\sin(a-|\theta|) + \frac{\ddot{u}_g}{g}\cos(a-|\theta|)\right]}^{frame\ system} \overbrace{-p^2 q\begin{bmatrix} k\operatorname{sgn}(\theta)\left(\sin\alpha - \sin(a-|\theta|) - \frac{u_{joint}}{2R}\right) \\ \cos(a-|\theta|) + c(\cos^2(a-|\theta|))\dot{\theta}\end{bmatrix}}^{abutment-backfill\ contribution}, \tag{18}$$

where $p = \sqrt{3g/4R}$ and $\gamma = m_{deck}/Nm_{pier}$ are the (known from the literature) parameters that describe the dynamic characteristics of the pier[18] and the influence of the mass of the superstructure on the rocking motion,[33] respectively. However, $q = 4R/g(Nm_{pier}+3m_{deck})$ is a new parameter that measures the longitudinal influence of the abutment-backfill system and depends on the properties of the bridge. It is noted that two distinct parts of Equation 18 contribute to the overall rocking response; the first one ("*frame system*") describes the motion before the deck contacts the abutments in the longitudinal direction, and it is exactly the same as the EoM of the symmetric rocking frame,[18] whereas the second term ("*abutment-backfill contribution*") is only active when the deck contacts the abutments longitudinally and describes the constraint of the framing system to the rocking motion due to the presence of the abutment-backfill system, that is, the interaction with the spring and the dashpot elements at each end of the deck is active. Considering two similar bridge configurations with the same properties for the abutment and the backfill at each bridge end (i.e., same values for spring stiffness k and dashpot coefficient c), the longitudinal influence of the abutment-backfill system depends entirely on the parameter q; large values of q indicate that the rocking system interacts with the abutment and the backfill to a significant extent, whereas for lower values, the response approaches that of the rocking frame addressed in previous studies (i.e., the "*frame system*" contribution dominates the EoM).[18] In order to illustrate the effect of the bridge characteristics on the contribution of the abutment-backfill system longitudinally, Figure 2A,B plots the value of q in terms of the size and number of piers (R and N, respectively) as well as the superstructure effect (γ), assuming same parameters for the abutment and the backfill at each end of the bridge. The results indicate that larger sections of the members (i.e., higher values of R and γ) and longer bridge structures (i.e., larger N) minimise the influence of the abutment-backfill system. Hence, without lack of generality, the greater the total mass of the bridge system, the lower is the engagement of abutment-backfill system longitudinally in the rocking response, reducing the rocking motion to that of an equivalent frame. It is also observed that for low values of all the examined parameters, small variations can change significantly the participation of the abutment-backfill system in the rocking response, whereas the value of q becomes almost constant when R, γ or N, are large.

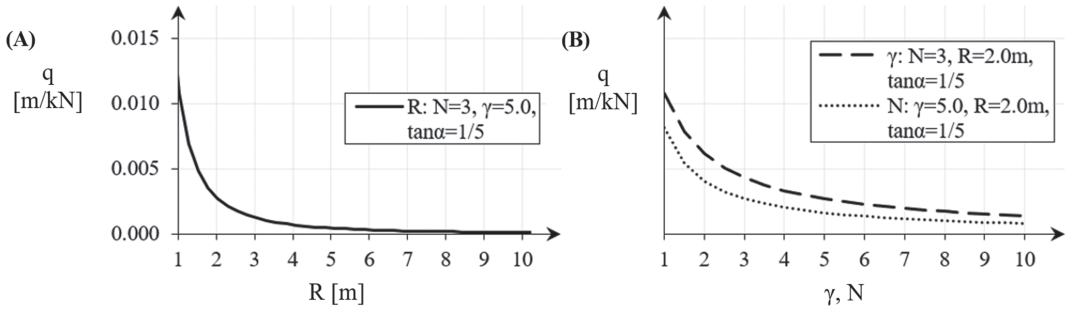

FIGURE 2 Longitudinal influence of the abutment-backfill system expressed in terms of the proposed parameter q for different values of (A) size of piers (R), (B) superstructure mass effect (γ) and number of piers (N)

2.4 | Impact formulation

When a rocking structure starts and sustains a pure rocking motion without overturning, Equation 18 describes the response-history of the angle of rotation (θ) of the piers; when $\theta = 0$, impact at the rocking interfaces occurs. These impacts dissipate energy instantly, and subsequently, the sign of the angle of rotation changes and its velocity reduces according to the coefficient of restitution $\eta = \dot{\theta}_2/\dot{\theta}_1$, where $\dot{\theta}_1$ and $\dot{\theta}_2$ are the angular velocities before and after the impact, respectively. From the energy balance perspective, the potential energy stored in the system (Equation 12) is zero immediately before and after the instant when impact occurs. Hence, at these two instants, the total energy in the system is all in the form of kinetic energy (Equation 10) which is subsequently dissipated. The ratio of energy loss due to impact is equal to $1 - \eta^2$. In the simple case of rocking of a free-standing column impacting on a rigid surface, the value of η depends solely on its slenderness (α).[15] In a symmetric rocking frame, η also depends on the mass of the cap beam represented by the parameter γ.[18] Equations for η in these cases are based on the assumptions of smooth change of rotation without bouncing or sliding, and on conservation of angular momentum during impact. These assumptions are only valid for slender columns[34] and for large coefficients of friction.[35] Furthermore, a "pointwise" approach was adopted by considering that the impact forces are concentrated at the corresponding pivot points, thus ignoring the potential migration of the resultant force towards the centre of the pier base due to an extended contact surface.[36] The present study follows an impulse approach based on the preceding assumptions, the novelty consisting in that it integrates in the mathematical development and in the resulting formulation of η the effect of the abutments acting as vertical supports and the length of end and intermediate spans.

To assess the postimpact state in the case of rocking, the impact problem presented in Figure 3 needs to be solved. The postimpact angular velocity of the piers is the variable to be determined ($\dot{\theta}_2$) and, therefore, the impact problem is treated in terms of impulses rather than forces. With reference to Figure 3, consider that all piers initially rock about pivots A′ and C′ in the counterclockwise (negative) direction with a magnitude of the angular velocity $\dot{\theta}_1$ and reverse the rocking rotation smoothly to the clockwise (positive) direction with angular velocity $\dot{\theta}_2$, now rotating around pivots A and C. At the intermediate condition, where the bridge is at the at-rest position, the abutments work as vertical supports (E and E′) and redistribute the deck weight when an impact is imminent. Hence, additional impulses (i.e., Λ_{Ex}, Λ_{Ez} and $\Lambda_{E'x}$, $\Lambda_{E'z}$) originate at the abutment seats, which do not occur in the rocking frames studied in previous works.[18] As a result, there are nine unknowns that need to be determined, namely, the impulses at the pivot points A of the two-side rocking piers in the longitudinal and vertical directions (Λ_{Ax} and Λ_{Az}), the impulses at the pivot points C of the $(N - 2)$ intermediate rocking piers in both directions (Λ_{Cx} and Λ_{Cz}) and those at the two abutment seats (Λ_{Ex}, Λ_{Ez} and $\Lambda_{E'x}$, $\Lambda_{E'z}$), as well as the angular velocity after impact ($\dot{\theta}_2$). Without lack of accuracy, static conditions are assumed

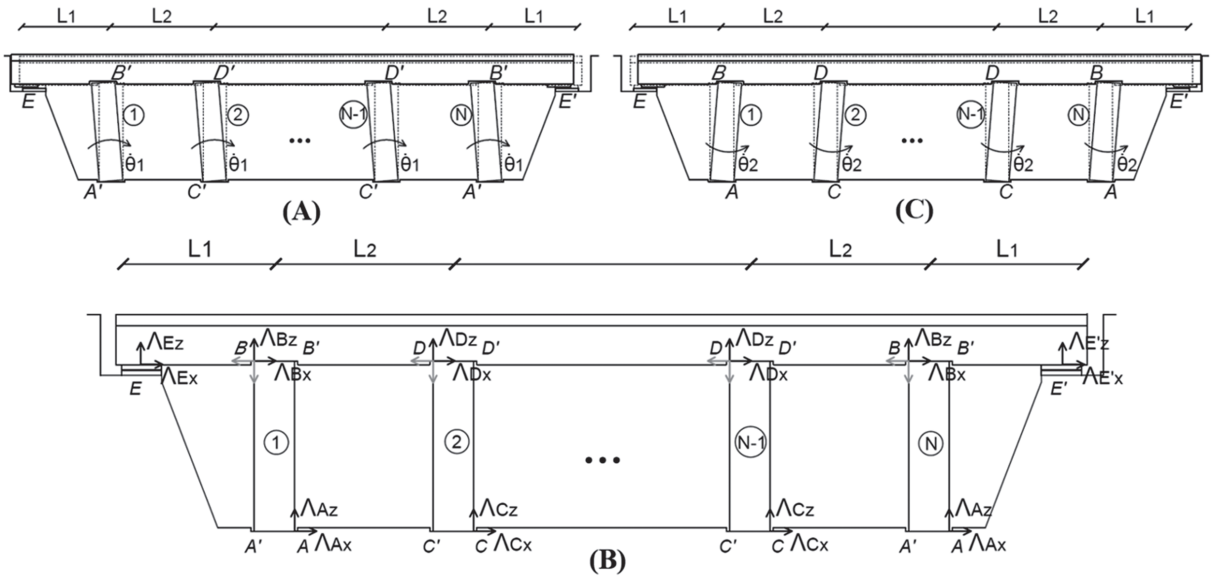

FIGURE 3 Impact problem considered in the rocking motion of a symmetric bridge that undergoes (A) counterclockwise (negative) rotation, (B) impacts at the pertinent pivot points and then reverses to (C) clockwise (positive) rotation

instantly when $\theta = 0$ after rocking is initiated. In addition, the assumptions of rigid deck and prevention of sliding at all the impact faces are made, which yield the following expressions

$$\Lambda_{Ex} = \Lambda_{E'x} = \frac{L_1}{L_1 + L_2}\Lambda_{Bx} \text{ and } \Lambda_{Ez} = \Lambda_{E'z} = \frac{L_1}{L_1 + L_2}\Lambda_{Bz}, \tag{19}$$

$$\Lambda_{Bx} = \frac{L_1 + L_2}{2L_2}\Lambda_{Dx} \text{ and } \Lambda_{Bz} = \frac{L_1 + L_2}{2L_2}\Lambda_{Dz}. \tag{20}$$

Equations 19 and 20 are used separately in order to reduce the number of unknowns in the impact problem. More specifically, the utilisation of Equation 19 and the conservation of linear momentum just before and after the impact along the X and Z axes for the side piers establishes the relationships between the impulses at the pivot points E and E′ with those at A

$$\Lambda_{Ex} = \Lambda_{E'x} = \frac{L_1}{L_1 + L_2}\left(\Lambda_{Ax} - m_{pier}H\left(\dot{\theta}_1 - \dot{\theta}_2\right)\right) \text{ and } \Lambda_{Ez} = \Lambda_{E'z} = \frac{L_1}{L_1 + L_2}\left(\Lambda_{Az} + m_{pier}B\left(\dot{\theta}_1 + \dot{\theta}_2\right)\right), \tag{21}$$

whereas Equation 20 combined with the conservation of linear momentum in both directions for the side and the intermediate piers relates the impulses at the pivots C and A

$$\Lambda_{Cx} = \frac{2L_2}{L_1 + L_2}\Lambda_{Ax} - \frac{L_2 - L_1}{L_1 + L_2}m_{pier}H\left(\dot{\theta}_1 - \dot{\theta}_2\right) \text{ and } \Lambda_{Cz} = \frac{2L_2}{L_1 + L_2}\Lambda_{Az} + \frac{L_2 - L_1}{L_1 + L_2}m_{pier}B\left(\dot{\theta}_1 + \dot{\theta}_2\right). \tag{22}$$

Equations 21 and 22 reduce the unknowns of the impact problem from nine to only three (Λ_{Ax}, Λ_{Az} and $\dot{\theta}_2$). Hence, the following equations are considered in the determination of these unknowns;

1 Linear momentum along X axis for the whole bridge:

$$\Lambda_{Ex} + 2\Lambda_{Ax} + (N-2)\Lambda_{Cx} + \Lambda_{E'x} = \left[Nm_{pier} + 2m_{deck}\right]H\left(\dot{\theta}_1 - \dot{\theta}_2\right). \tag{23}$$

2 Linear momentum along Z axis for the whole bridge:

$$\Lambda_{Ez} + 2\Lambda_{Az} + (N-2)\Lambda_{Cz} + \Lambda_{E'z} = -\left[Nm_{pier} + 2m_{deck}\right]B\left(\dot{\theta}_1 + \dot{\theta}_2\right). \tag{24}$$

3 Angular momentum at point B for a side pier:

$$2H\Lambda_{Ax} + 2B\Lambda_{Az} = \left[-I_{pier}^{CG} + m_{pier}H^2\right]\left(\dot{\theta}_1 - \dot{\theta}_2\right) - m_{pier}B^2\left(\dot{\theta}_1 + \dot{\theta}_2\right). \tag{25}$$

Equations 23 to 25 describe the impact problem when the rotation changes from negative to positive. In the opposite case (rocking from positive to negative rotation), the problem is treated in a similar way, but the equations are not presented here, for brevity. The coefficient of restitution in the rocking motion of the bridge, $\eta = \dot{\theta}_2/\dot{\theta}_1$, is obtained by solving the system of Equations 23 to 25

$$\eta = \frac{\dot{\theta}_2}{\dot{\theta}_1} = \frac{1 - \frac{3}{2}\sin^2 a + \frac{3}{2}(\bar{L}+1)\gamma\cos 2a + \frac{1}{4N}((2\bar{L}-1) + (6\bar{L}-3)\cos 2a)}{1 + \frac{3}{2}(\bar{L}+1)\gamma + \frac{1}{N}(2\bar{L}-1)}, \tag{26}$$

and η is independent of the direction of the rocking movement due to the symmetry of the rocking system. Equation 26 includes an additional dimensionless factor $\bar{L} = L_1/L_2$ which is not present in the restitution coefficient for a rocking frame with the same number of columns and describes the effect of the span arrangement in the bridge. If $L_1 = L_2$ (then $\bar{L} = 1$), the span arrangement has no effect on the impulses developed at each pier, and the impulses in both directions at the foundation level are the same for all piers (i.e., $\Lambda_{Cx} = \Lambda_{Ax}$ and $\Lambda_{Cz} = \Lambda_{Az}$). If, in addition, the impulses that are developed at the abutments are ignored by introducing $\Lambda_{Ex} = \Lambda_{Ez} = \Lambda_{E'x} = \Lambda_{E'z} = 0$ in Equations 23 and 24, the coefficient η reduces to the simpler one derived in previous works for rocking frames.[18]

$$\eta = \frac{\dot{\theta}_2}{\dot{\theta}_1} = \frac{1 - \frac{3}{2}\sin^2 a + 3\gamma\cos 2a}{1 + 3\gamma}. \tag{27}$$

As it was mentioned previously, the differences between the value of η in rocking bridges and rocking frames stem from the impact at the vertical supports of the abutment seats and from the span arrangement in the bridge. Figure 4 depicts the effect of the additional impacts at the ends of the bridge deck by ignoring the effect of the side spans (i.e., $\bar{L} = 1$) and compares η in rocking bridges and in frames with equivalent dimensions. The results are for structures with four rocking piers ($N = 4$) with slenderness $a = 0.165$ rad, for different values of superstructure effect γ. It is apparent from Figure 4 that the value of the coefficient of restitution for the rocking bridge is always higher than that for the corresponding frame for any value of γ. This means that the energy dissipation associated with each impact at the rocking interfaces is always lower in the bridge and this is due to the redistribution of the weight of the superstructure by the abutments, which reduces the weight supported by each pier. Furthermore, the value of η for bridges is lower for larger values of γ, confirming the beneficial effect of heavier superstructures on rocking attenuation which is consistent with previous findings.[33] It should be noted that although the difference between the value of η in bridges and frames is relatively small (below 1% for all the examined cases), rocking stability can be considerably differentiated due to the highly nonlinear nature of rocking response.

Compared with the simple rocking frame case, the attenuation of the rocking motion at each impact at the rocking interfaces (η) for a bridge depends on a number of additional parameters, namely, the length of the bridge spans (L_1 and L_2) as well as the number of piers (N). To better understand the effect of these parameters on the value of η, reference is made to a bridge with constant deck mass $m_{deck} = 2.7 \cdot 10^6$ kg that is supported on rectangular piers with the same dimensions $2B = 3$ m and $2H = 15$ m for all the examined cases. Figure 5A shows that longer end spans (L_1) with constant length for the intermediate spans (L_2) result in higher values of η because the vertical reaction forces at the piers are smaller (they are larger at the abutment seats), which reduces the energy loss at every impact at the rocking interfaces during the rocking motion. The opposite occurs if the length of the intermediate spans (L_2) is increased keeping constant the length of the end spans (L_1), which leads to slightly larger energy dissipation and smaller η, as shown in Figure 5B. The influence of the increasing number of piers keeping the mass deck constant is represented in Figure 5C. It can be observed that distributing the constant weight of the deck to more supporting piers leads to larger values of η based on the same reasoning. As expected, the effect of number of piers N is more significant than changing the span arrangement, as it is observed in the shifting of the curves in Figure 5A,B and the steeper slope of the curves in Figure 5C.

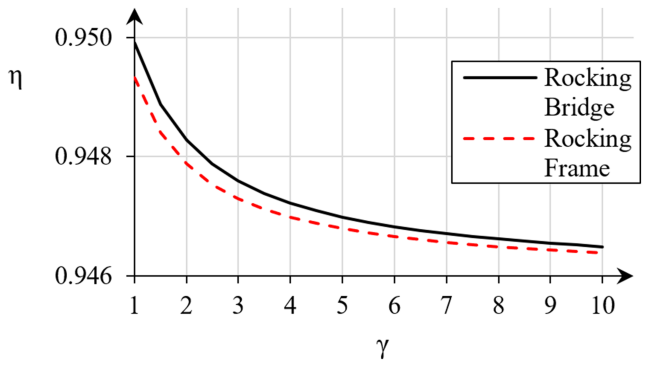

FIGURE 4 Comparison between coefficient of restitution (η) for rocking bridges and frames in which $\bar{L} = 1$ considering different values of the superstructure effect (γ). Case with $N = 4$ and $a = 0.165$ rad [Colour figure can be viewed at wileyonlinelibrary.com]

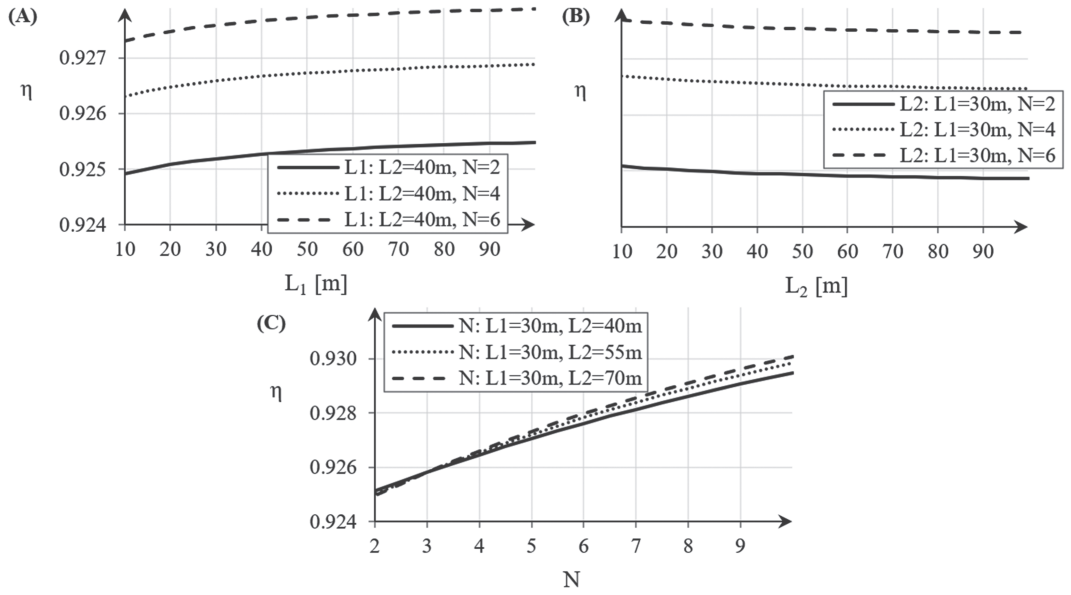

FIGURE 5 Influence of (A) the length of end (L_1) and (B) intermediate spans (L_2) as well as (C) the number of piers (N) on the restitution coefficient (η) for symmetric bridge structures. Cases with constant deck mass

It must be noted that the influence of impact at the rocking interfaces depends on additional factors that are not considered in the development of Equation 26, such as the magnitude of the angular velocity,[37] the inelastic behaviour of the interface material[38] and the imperfections of the contact surfaces[39]; moreover, this study neglects the influence of the impacts of the superstructure on the abutment backwalls which occur instantaneously and lead to additional energy dissipation (i.e., pounding).[40,41] Thus, the proposed value of η represents an upper bound to the total energy dissipated for a rocking bridge system, therefore, rendering the analytical modelling presented as conservative.

3 | CONTRIBUTION OF THE ABUTMENT-BACKFILL SYSTEM IN THE ROCKING OF BRIDGES

In order to assess the safety of rocking bridges accounting for the abutment-backfill system, a new failure criterion has to be introduced based on the risk of damage or collapse due to excessive longitudinal displacement of the deck at the abutments. The abutment-backfill system fails if the longitudinal displacement of the superstructure (u_{deck}^{CG}) closes the end joint gap (u_{joint}) and induces a displacement at the abutments that exceeds their capacity ($u_{abut.}$). This failure mode can be expressed in terms of the DOF of the rocking system (θ) by rearranging Equation 3

$$u_{deck}^{CG} = \mathrm{sgn}(\theta)\left(u_{joint} + u_{abut.}\right) \Leftrightarrow \theta_{abut.} = \mathrm{sgn}(\theta)\left[a - \sin^{-1}\left(\sin a - \frac{u_{joint} + u_{abut.}}{2R}\right)\right]. \tag{28}$$

Several proposals can be found in the literature regarding the capacity of abutments and backfills or entire embankments including collapse of the abutment-backfill system due to exceedance of shear strength of the abutment backwall (e.g., Kwon and Elnashai[42]), failure of abutment foundation or "unrecoverable abutment damage" (e.g., Kappos et al.[28]) and unseating of the deck due to large displacements and/or inadequate seat lengths; the latter is typically prevented when bridges are designed according to modern code provisions (e.g., previous study[43]). However, in the context of the present study, the failure criterion to be used for these systems needs to be comparable with the

overturning criterion used for the rocking piers (i.e., $\theta_{over.} = \text{sgn}(\theta)\ a$) which is physical collapse, and hence relates to Collapse Prevention in performance assessment. Simplified approaches like exceedance of shear strength of the abutment backwall[42] can considerably underestimate the overall seismic performance of bridges compared with refined approaches like that considering the behaviour of a specific abutment-backfill system in the nonlinear range using a "full-range" pushover analysis up to significant drop in strength.[28] This is due to the fact that the latter recognises that backwalls are sacrificial elements that may fail under large ground motions, but there is no system failure so long as the abutment transfers the horizontal loads from the deck to the backfill. Thus, additional horizontal loads can be accommodated by the abutment-backfill system after "failure" of the backwall. On the contrary, failure of the abutment foundation[28] can be considered as system failure, broadly equivalent to overturning of the rocking piers. Hence, this study points to the need of properly defining the behaviour of the abutment-backfill system in the rocking problem while small variations in the values of spring stiffness (k), dashpot coefficient (c) and displacement capacity of the abutment-backfill system ($u_{abut.}$) can affect significantly the safety of rocking bridges and, therefore, it is important to account for failure of these components in performance assessment. In addition to the abutment failure criterion, the "traditional" overturning criterion of the rocking piers is also considered, that is, pier overturning occurs only when the total mass of the system can no longer act as a restoring mechanism. This condition is achieved when the longitudinal displacement of the pier exceeds the overturning threshold (i.e. $\left|u_{pier}^{CG}\right| > B$), or the displacement of the superstructure exceeds double of this value (i.e., $\left|u_{deck}^{CG}\right| > 2B$). The dominant failure mode of the system is established by the properties of the bridge structure. Hence, the abutment-backfill member fails first as long as $|\theta_{over.}| > |\theta_{abut.}|$ or $2B > u_{joint}+u_{abut.}$, whereas overturning prevails if $|\theta_{over.}| < |\theta_{abut.}|$ or $2B < u_{joint}+u_{abut.}$; as expected, simultaneous failure of the entire system occurs when $\theta_{over.} = \theta_{abut.}$.

The abutment-backfill contribution in rocking response is studied here by comparing the seismic performance of two rocking bridges (one with a short/light configuration and the other with a long/heavy one) with that of the corresponding rocking frames without abutments at the ends of the superstructure, using both single-frequency and multi-frequency ground motions. The structures have a total length $L_{tot} = 2L_1+2L_2 = 2 \cdot 50+2 \cdot 50 = 200$ m and $L_{tot} = 2L_1+6L_2 = 2 \cdot 50+6 \cdot 50 = 400$ m, and they are supported on $N = 3$ and $N = 7$ rocking piers of rectangular cross-section, respectively, leading to a total mass $m_{tot} = 3.1 \cdot 10^6$ kg and $m_{tot} = 7.2 \cdot 10^6$ kg, respectively. The superstructure in both configurations consists of a single-cell box girder with depth $2h = 1.7$ m, whereas the width of the bottom and the top slabs of the deck are $B_{bot} = 6$ m and $B_{top} = 9.5$ m, respectively. The flange ($t_f = 0.25 - 0.3$ m) and the wall thicknesses ($t_w = 0.7 - 0.8$ m) of the box girder section were adjusted with a view to achieving a mass ratio equal to $\gamma = 4.8$ for both rocking structures. The deck has a constant section with cross-sectional area $A_{deck} = 5.2$ m^2 and $A_{deck} = 6$ m^2 for the light and the heavy system, respectively. The piers have a width $2B = 1.8$ m and a height $2H = 22$ m for both configurations. The length of the end joint gaps depends on both service loads (shrinkage, creep, temperature, prestressing) and the seismic demands. To check the effect of the joint length (u_{joint}) on the seismic response of the rocking bridges, a parametric analysis with respect to the length of the joint was conducted for the heavy configuration (i.e., with $N = 7$ rocking piers). Three different lengths were considered, 0.1 m, 0.15 m, and 0.2 m. It was observed that the effect of the end gap size on the rocking response of the bridge configuration with $N = 7$ piers is significant, with larger end gaps leading to reduced longitudinal stiffness and, therefore, resulting in larger longitudinal displacements of the deck compared with the systems with lower end gaps. For the parametric studies, a relatively large longitudinal joint gap equal to 0.1 m and 0.15 m for the short and the long bridge, respectively, was selected. The abutment properties of an actual overpass, part of the Egnatia Motorway (Greece)[28] were selected for both bridge configurations with total height $H_{abut.} = 5.5$ m and width $B_{abut.} = 10.5$ m, whereas the height and the thickness of the backwall were $h_{bw} = 2$ m and $b_{bw} = 0.4$ m, respectively. The present study adopts the mechanical properties of a typical backfill from well-compacted sand with friction angle $\varphi = 40^o$ classified as ground C ($V_{s,30} \approx 270$ m/s) according to EC8 site classification.[43] The values for spring stiffness (k) and displacement at failure of the abutment-backfill system ($u_{abut.}$) are derived from the corresponding pushover curve in the longitudinal direction, considering that subsequent to pier yielding the end gap closes, and thereafter, the pushover curve is dominated by the behaviour of the abutment and the backfill. Figure 6 shows the bilinear behaviour of the abutment-backfill system. For the sake of simplicity, the equivalent linearisation approach based on the secant stiffness is selected for the spring stiffness of the abutment-backfill system. The most conservative value for secant stiffness is defined from the pushover curve at the ultimate displacement, leading to $k = 132$ MN/m, whereas the displacement at failure of the abutment-backfill system is $u_{abut.} = 0.1$ m. It is noted that this spring stiffness is consistent with Caltrans recommendations.[44] Following the work of Mylonakis et al.[45] the dashpot coefficient that represents both radiation and material damping of the backfill soil is $c = 44$ MN s/m.

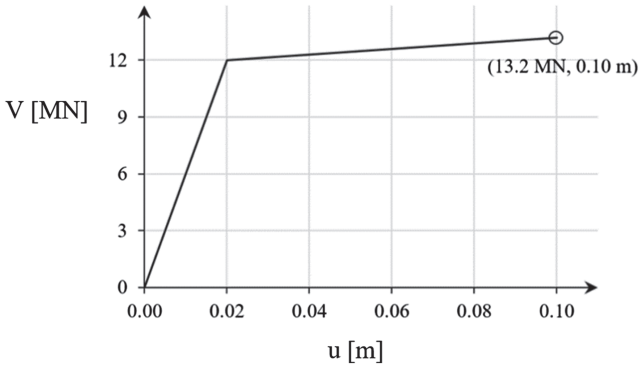

FIGURE 6 Force-displacement behaviour of the abutment-backfill system in the longitudinal direction[28]

3.1 | Single-frequency pulse-type ground motions

This section addresses the effect of the abutment-backfill system on the seismic performance of symmetric rocking bridges considering pulse-type excitations. This type of motions that are described by simple mathematical expressions can capture both qualitatively and quantitatively the most destructive part of near-fault ground motions to which rocking structures have shown high vulnerability (e.g., Kirkpatrick[46]). A useful way of illustrating the vulnerability of rocking structures in such pulses is with spectra constructed for the minimum acceleration amplitude, a_p, of the pulse-type motion with given angular frequency, ω_p, that is able to induce failure for a rocking structure with vertical members of certain frequency parameter, p, and slenderness, α. The resulting graph divides the possible combinations of the seismic intensity and the structural characteristics in two areas, one wherein the structure fails and the other one that delineates a safe area; the unsafe area consists of smaller regions described by the number of impacts before failure (i.e., failure occurs without experiencing any impact before failure or after the rocking structure exhibits one or more impacts[16]) which will not be examined herein. These graphs are generalised by utilising dimensionless variables (i.e., ω_p/p, $a_p/\mathrm{gtan}\alpha$) which offer a physically self-similar description of the response for a broad range of structures with equivalent characteristics.[47] In this work, the ground motion is defined by three different mathematical excitations, which have shown good agreement with near-fault ground motions,[18,48] namely, sine, Ricker symmetric and antisymmetric pulses, as described by Equations 29 to 31, respectively

$$\ddot{u}_g(t) = a_p \sin\left(\frac{2\pi}{T_p}t\right), \tag{29}$$

$$\ddot{u}_g(t) = a_p\left(1-\frac{2\pi^2t^2}{T_p^2}\right)\exp\left(-\frac{1}{2}\frac{2\pi^2t^2}{T_p^2}\right), \tag{30}$$

$$\ddot{u}_g(t) = \frac{a_p}{\beta}\left(\frac{4\pi^2t^2}{3T_p^2}-3\right)\frac{2\pi t}{\sqrt{3}T_p}\exp\left(-\frac{1}{2}\frac{4\pi^2t^2}{3T_p^2}\right), \tag{31}$$

where $T_p = 2\pi/\omega_p$ is the period of each pulse-like motion and $\beta = 1.38$ in Equation 31 maximises the function to the acceleration amplitude a_p. The first studies using this type of analysis examined blocks or frames and defined overturning as the only failure mechanism of the system, and, therefore, their outcome is commonly referred to as Overturning Minimum Acceleration Spectra (OMAS).[16,18] However, the term OMAS cannot describe the more complex nature of the failure of rocking bridges, and a broader term is used in the following to capture this: Failure Minimum Acceleration Spectra (FMAS).

Figure 7 presents the FMAS for the bridges and their equivalent rocking frames. The bridges are designed to be more susceptible to fail due to high demand of longitudinal displacement at the abutments than due to overturning of the piers; this is because $2B = 1.8$ m $> u_{joint}+u_{abut.} = 0.2$ m and $2B = 1.8$ m $> u_{joint}+u_{abut.} = 0.25$ m in the short and in the long bridge, respectively. However, in order to examine the influence of the abutment-backfill system on the response in more detail, both failure modes for bridges (i.e., abutment failure as per Kappos et al.[28] and overturning)

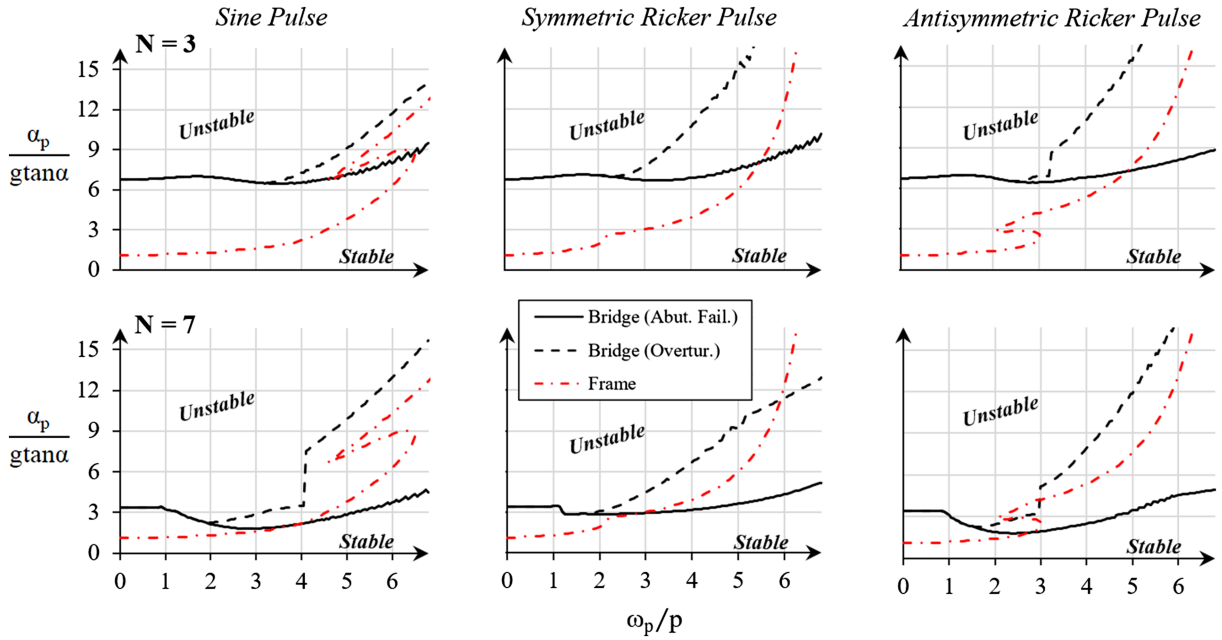

FIGURE 7 Failure Minimum Acceleration Spectra (FMAS) for the symmetric rocking bridges and for the frames with $N = 3$ and $N = 7$ piers. The structures are subjected to acceleration pulses of sine, symmetric and antisymmetric Ricker type [Colour figure can be viewed at wileyonlinelibrary.com]

are plotted in the failure graphs of Figure 7 and are compared with the overturning condition of the equivalent frames without abutments. These failure spectra are constructed by obtaining the response-history response of the pier rotation (θ) for different values of the dimensionless parameters ω_p/p and $a_p/\text{gtan}\alpha$. For any given pulse-like ground motion and rocking properties of the structure, Equation 8 is used to determine the moment at which the bridge (or frame) starts rocking, and Equation 18 (only "*frame system*" when the rocking frame is considered) is integrated step-by-step using the ode45 solver in MATLAB[49] with a time-step of 10^{-3} seconds. The response-history solution of the EoM requires identifying the instants at which $\theta = 0$ after rocking initiation. At these instants, impacts at the rocking interfaces occur, and Equation 26 (or Equation 27 when the rocking frame is examined) is employed to account for the corresponding attenuation of the rocking motion. A wide range of pulse durations and acceleration amplitudes are considered to obtain a broad view of the risk of failure for different scenarios. The ground motion parameters are scaled gradually with respect to the rocking properties, that is, for pulses of constant angular frequency $\omega_p = [0.1 - 6] \cdot p$ (and $p = 0.82$ rad/s), the acceleration amplitude $a_p = [0.1 - 15] \cdot \text{g tan}\alpha$ (and g tan$\alpha = 0.082$ g) is gradually increased to determine the minimum acceleration capable of inducing failure. As expected, the overturning behaviour for the rocking frames is predictable, showing high vulnerability to low-frequency acceleration pulses, which is gradually decreased for medium and high-frequency pulses as also found in previous works ([18,19] among others). However, compared with frames, the seismic performance of the studied bridges against pier overturning is differentiated, revealing highest sensitivity to medium-frequency pulses (2–4 Hz for the bridge with $N = 3$ piers and 1–4 Hz for the bridge with $N = 7$ piers, depending on the shape of the pulse-type motion). Moreover, the hitherto ignored failure mode at the abutments modifies the failure spectrum of rocking structures to one that can be described as "sickle" shaped, depending on the total mass of the structure. Specifically, the curves representing collapse for the bridge systems show that failure of the abutments and overturning coincide over a considerable range of frequency pulses (up to approximately 3.5 Hz for the bridge with $N = 3$ piers and up to 2 Hz for the bridge with $N = 7$ piers), implying that the same pulse-like ground motion is able to induce either failure mode. Interestingly, within this low-frequency range, the FMAS for the bridges present a straight branch (up to 1 Hz for both bridges independently of the pulse type) which is followed by a zone in which the critical acceleration decreases with increasing ω_p/p, especially for the heavy configuration. This type of behaviour is not observed in the corresponding rocking frames. The straight branch in the FMAS for bridges shows critical acceleration amplitudes that are up to six and three times higher than those for the frames for the light and heavy structure, respectively, while the decreasing zone approaches the overturning behaviour of the frames, especially for the heavy structure. After that point and as expected from the foregoing discussions about the prevailing failure mode

of the bridges, the minimum acceleration amplitude that activates pier overturning increases with ω_p/p at a much higher rate than that for abutment failure, which is less sensitive to the dimensionless frequency parameter ω_p/p. For this reason, the minimum acceleration that induces overturning in the piers is up to five times larger than that for abutment failure in the high-frequency region for both bridge configurations. It is interesting to note that the abutment failure mode governs the overall seismic instability in the range of medium and high-frequency acceleration pulses (after 5 Hz for the light structure and after 3 Hz for the heavy one, depending on the type of pulse-type motion). Hence, there are cases where the overturning mode of the frame model overestimates bridge safety compared with the abutment failure, and this study highlights the need for accounting for all expected failure modes in rocking bridges. Nevertheless, by examining pier overturning of the bridge structures notwithstanding abutment failure, the beneficial influence of the abutment-backfill system in preventing overturning in rocking bridges compared with frames is also observed; opposite trends appear for the heavy system, though, when high-frequency symmetric Ricker pulses of large magnitude are considered which do not really change the picture of the improved behaviour of bridges against overturning, as they occur only for extreme conditions. To check whether consideration of pounding would affect the findings of this study, a more involved analytical model was set up for the rocking bridge considering the pounding effect between superstructure and abutment backwall. This was made by means of the "stereomechanical" approach,[40] using a restitution coefficient e = 0.6[50–52] which expresses the attenuation of superstructure's movement during impact. This model resulted in reduced deck displacements for the rocking bridge compared with those found neglecting deck pounding, and corresponding upward shift of the bridge failure curves (FMAS) shown in Figure 7 (including those related to the failure of abutments and overturning), independently of the mass of the system and the type of ground motion. Nevertheless, this reduction in the peak deck displacements was only up to 5% compared with the system ignoring pounding and, therefore, it did not affect the findings discussed earlier.

Figure 7 also indicates that a self-similar response is achieved for the frame systems when subjected to pulses of the same form (i.e., with $B = 0.9$ m, $H = 11$ m and $\gamma = 4.8$ for both frame configurations, the overturning curves are exactly the same regardless of the total mass or length of the structure). However, the overturning curves of the light ($N = 3$ piers) and heavy bridge ($N = 7$ piers) are different when pulses of the same type are examined, which is attributed to the influence of the total mass of the system on the abutment-backfill parameter q. Specifically, a larger overturning zone appears for the heavy bridge than for the light one. According to Figure 2, the light bridge is expected to interact to a higher extent with the abutment-backfill system than the heavy bridge because its parameter q is lower ($q = 5.5 \cdot 10^{-4}$ m/kN in the light bridge and $q = 2.3 \cdot 10^{-4}$ m/kN in the heavy one), which implies that its response is closer to that of the frame. Accordingly, the light bridge is safer than the heavy one when abutment failure is considered for same type of pulse motion. Hence, self-similarity in bridge structures can be accomplished only if different properties for the abutment and the backfill are selected in relation to the weight of the corresponding configuration (e.g., for the heavy bridge examined, larger abutment dimensions or stiffer backfill soil should be selected a priori leading to larger values for k and c to counteract the decreased value of q compared with the light system). To this end, joint gaps (u_{joint}) with the same length are also required for the different configurations, highlighting even more the complexity of the rocking problem in bridges. Consequently, rocking bridges cannot achieve self-similar response in the context adopted so far (i.e., structures with same values for B, H and γ independently on the total mass of the structure) due to the fact that different values must be selected for the spring stiffness (k) and dashpot coefficient (c) which should be directly proportional to the influence of the abutment-backfill system (q). Thus, the FMAS for bridges differs in principle from that for frames due to the presence of the abutment-backfill system, making the rocking response of this system more nonlinear.

3.2 | Multi-frequency synthetic ground motions

The present section extends the seismic performance analysis of the same symmetric rocking bridges and frames subject to acceleration response-histories composed of a wide range of frequencies. The seismic action is represented by ten artificial excitations[53] with Peak Ground Acceleration (PGA) 0.41 g and total duration 25 seconds, generated to fit the reference EC8 target spectrum[43] considering PGA equal to 0.36 g and site conditions C; note that this PGA is the highest one currently prescribed in Southern Europe. Figure 8 presents the fit of the individual artificial records and their geometric mean (GM) to the target Eurocode 8 spectrum.

The two rocking bridges and the equivalent frames are subjected to the ten artificial ground motions. Figure 9 illustrates the peak responses of the superstructure longitudinal displacement (u_{deck}^{CG}) for the rocking structures with $N = 3$

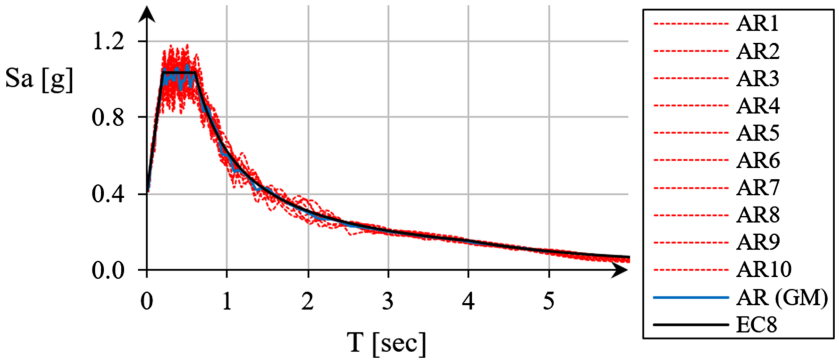

FIGURE 8 Response acceleration spectra of the set of artificial records and matching to Eurocode 8 target spectrum with Peak Ground Acceleration (PGA) = 0.36 g

and $N = 7$ piers; the displacement corresponding to contact with the abutments (dotted line) as well as the ultimate displacement demand in the abutment-backfill systems (dashed line) are also shown for the bridge structure. As expected, due to the self-similarity in rocking response, the frame models for the light and heavy configurations present same peak responses independently of the total mass or length of the structure. It is observed that the frame system develops longitudinal displacements that are significantly larger compared with those in a bridge with abutments. On average, the frame system overestimates the rocking amplitudes in the corresponding light structure by 419%, and in the heavy structure approximately by 221%. The reduced overestimation for the heavy structure is attributed to the stabilising effect of the abutments, directly proportional to the decreased value of q, confirming the decreased contribution of the abutment-backfill system to the rocking performance of heavy (multi-span) bridges. Moreover, comparison in a performance assessment context reveals that the bridge and frame models do not trigger the prevailing failure modes of the abutment-backfill system and overturning, respectively, in any case. The lowest safety margin against the corresponding prevailing failure mode of each system is met for the heavy bridges against abutment failure and is approximated to a minimum of 23% for AR10 motion, contrary to the frame models and the light bridges where the pertinent values are 35% against overturning (i.e., 1800 mm ultimate superstructure capacity) for AR8 and 61% against abutment failure for AR6, respectively. Thus, slightly stronger ground motions could trigger abutment failure for the heavy bridges whereas the frame models could maintain their integrity, confirming that the frame system without abutments at the end of the superstructure misses potential failure modes, thus overestimating bridge safety. Additionally, longitudinal deck displacements higher than 700 mm as those met for the frame models are considered as extreme for the examined bridge structures under seismic design actions. It is also observed that the record-to-record variability of the response is much more significant in the frames than in the bridges, for which the peak response is almost unaffected by the randomness in the artificial record, particularly in the light bridge. Thus, it can be concluded that the frame model without abutments is not adequate for predicting in a comprehensive way the rocking response of real bridges because the contribution of the abutment-backfill system is crucial for assessing their performance. In view of the fact that a conservative value was adopted for the secant stiffness of the abutment-backfill system (i.e., that

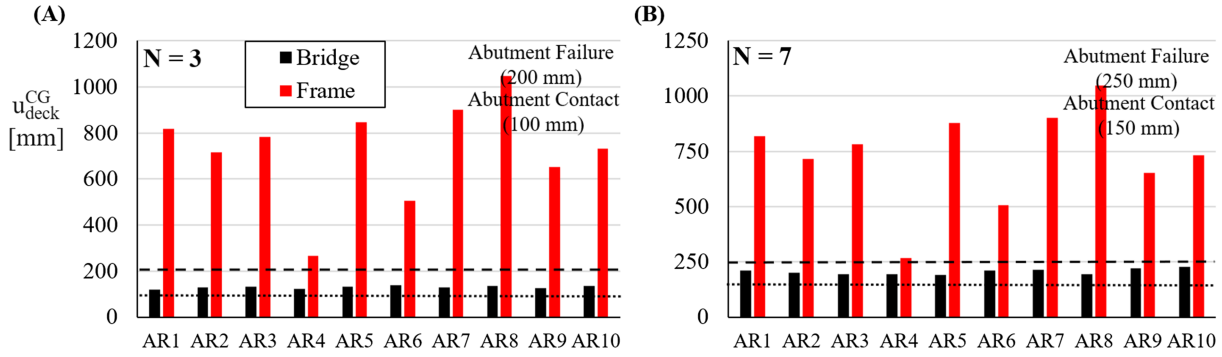

FIGURE 9 Peak responses of the longitudinal displacement of the superstructure (u_{deck}^{CG}) for the symmetric rocking bridges and for the frames subject to artificial earthquakes: (A) structures with $N = 3$ rocking piers, (B) structures with $N = 7$ rocking piers

corresponding to the abutment displacement at failure), a more refined approach for the determination of k was explored based on the secant stiffness at the displacement triggered by each ground motion (hence, an iterative approach was used). The results of these additional analyses showed that the refined approach can lead to deck displacements lower by up to 8% compared with the conservative approach adopted in the bulk of the analyses. Thus, the rocking frame model overestimates the deck displacements approximately 430% for the light bridge (with $N = 3$ piers) when adopting an updated secant stiffness of the abutment-backfill system, which is practically the same overestimation (i.e., 419% as mentioned before) with respect to the same bridge model with secant stiffness obtained for a target displacement of 0.1 m. Similar trends occur for the heavy configuration. Consequently, the key conclusion of this study regarding the overestimation of displacements by the rocking frame model does not change if a more refined procedure for secant stiffness is followed.

Figure 10 shows the response histories of the longitudinal displacement of the deck (u_{deck}^{CG}) for the rocking structures with $N = 3$ and $N = 7$ piers when subjected to two of the artificial records. Again, the displacements describing contact with the abutments (dotted line) and failure of the abutment-backfill systems (dashed line) are illustrated. It is observed that rocking initiates at $t \simeq 6$ seconds for both bridge and frame structures, independently of the effect of the abutments (i.e., rocking initiation is the same for bridges and frames following Equation 8). Similarly, and after rocking initiation, the results show that in the very first rocking cycles (i.e., up to $t \simeq 8$ seconds) the two structures behave the same way while the abutment-backfill system has not been activated and the free rocking motion prevails (i.e., the term "*frame system*" in Equation 18 dominates the EoM of the bridge structure). However, after that point, the results show that the response-history of the superstructure displacement in the frames, apart from revealing significantly larger rocking amplitudes than those in the bridges, it lasts much longer. In fact, the motion of the rocking bridges almost expires when the ground motion ceases (at $t \simeq 25$ seconds), whereas at the same time, the rocking frames experience some of the highest rocking amplitudes for the entire motion. The improved seismic behaviour of the bridges is attributed to the function of the abutment and the backfill from $t \simeq 8$ seconds to the end of ground motion ($t \simeq 25$ seconds), when the longitudinal movement of the deck is large enough to close the gap at the joints. In this interval, the bridge systems are constrained longitudinally by the abutment-backfill systems and are forced to return to the equilibrium position, dissipating energy at each contact with the abutments, whereas the frame systems are free to experience some large rocking amplitudes (exceeding 500 mm and 350 mm for the frames with $N = 3$ and $N = 7$ rocking piers, respectively). Thus, despite the slightly lower energy dissipation at each impact at the rocking interfaces for the bridges compared with the frames (the restitution coefficients are practically the same $\eta = 0.9869$ and $\eta = 0.9870$ for frame and bridge systems, respectively), the rocking motion of the systems accounting for the abutment-backfill behaviour is considerably suppressed compared with the frames. It is noted, though, that when accounting for abutment-backfill contribution, additional energy is dissipated at each contact of the superstructure with the abutments via the dashpot elements. Hence, the total energy dissipated by a bridge structure is (considerably) higher than that for a simple frame model. It is also important to note that the number of impacts at the rocking interfaces during the rocking motion, which can

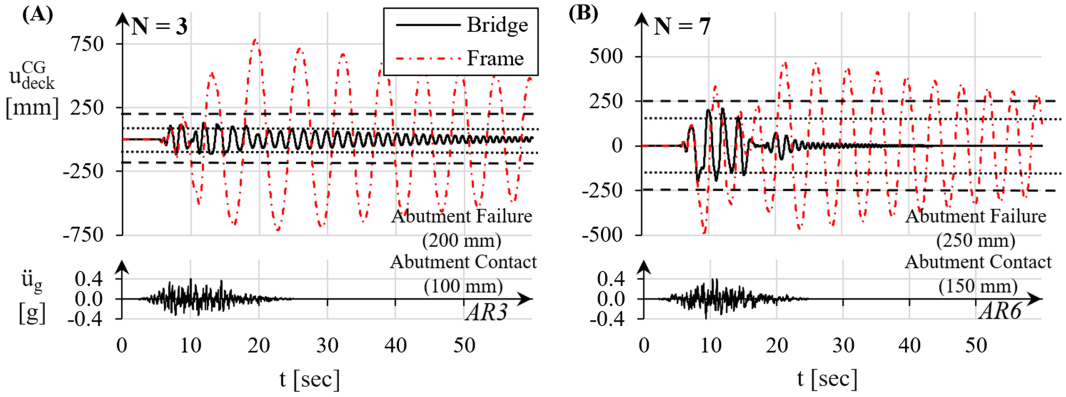

FIGURE 10 Response histories of the longitudinal displacement of the superstructure (u_{deck}^{CG}) for the symmetric rocking bridges and for the frames: (A) structures with $N = 3$ rocking piers subject to artificial AR3, (B) structures with $N = 7$ rocking piers subject to artificial AR6 [Colour figure can be viewed at wileyonlinelibrary.com]

damage the rocking interface and reduce the rocking stability,[54] is significantly reduced in the bridge structures compared with frames considering that the rocking motion of the latter expires at a later stage (not shown in Figure 10A).

4 | SUMMARY AND CONCLUSIONS

This study investigated the seismic response of symmetric rocking bridges, accounting for the first time for the influence of the abutment-backfill system. This is done by introducing a spring (k) and a dashpot (c) element at each end of the deck in the longitudinal direction, in addition to vertical supports at the abutment seats. The EoM accounts for the stages before and after the closure of the gap at the bridge end joints, when the spring and dashpot elements are activated. When this happens, a new parameter that describes the degree of influence of the abutment-backfill system (q) appears in the EoM of the rocking bridge (Equation 18). The results indicate that the lighter the structure, the higher the value of q is, indicating a stronger interaction with the spring and dashpot elements of the abutment-backfill system. The problem of impact at the rocking interfaces during the rocking motion of the bridge is formulated analytically using the concept of the restitution coefficient (η) based on the impulses developed at the different impact points, including for the first time the impulses at the abutments. A new expression for η is derived accounting for the length of the end and the intermediate spans, as well as the number of piers in the rocking bridge, which are parameters that do not affect the value of the corresponding rocking frame without abutments presented in previous works. The dissipated energy at each impact at the rocking interfaces for a bridge structure is always lower (higher value of η) than that of a rocking frame with equivalent characteristics due to the influence of the vertical supports of the abutments which carry part of the weight of the superstructure. However, additional energy is dissipated for the bridge structure when the deck contacts the abutments via the dashpot elements at each bridge end, indicating that the total energy dissipated for the bridge system is higher compared with the corresponding rocking frame without abutments. Hence, unlike previous works on the dynamics of rocking frames deemed to represent bridges, the present study shows that this approach is not comprehensive because the presence of seat-type abutments and backfills may considerably affect the dynamics of rocking bridges.

Previous works on rocking structures considered the overturning of the vertical supporting members as the only failure mode of the system. However, in bridges, an additional failure criterion has to be considered to describe failure of the abutment-backfill system, defined in a way consistent with failure due to overturning of the rocking piers. To incorporate failure of the abutment-backfill system in the assessment of rocking bridges, the existing overturning spectra for pulse-type motions (OMAS) were extended here to the so-called Failure Minimum Acceleration Spectra (FMAS). Two conventional bridges with equivalent characteristics (i.e., same B, H and γ for all the cases) were selected in an effort to establish the effect of the abutment-backfill parameter (q) on rocking response. The results for the rocking bridges obtained via FMAS show that the structure with higher interaction with the abutment-backfill system (i.e., higher value for q, or lighter system) is safer than the corresponding heavier configuration, when same properties are considered for the abutment, the backfill and the end joint at each bridge end. Thus, self-similarity in bridge structures cannot be achieved in the context adopted so far for frame models and, therefore, the FMAS differ from the corresponding OMAS both in terms of the failure modes depicted on the graph and on the basic rules on which the seismic stability of rocking structures is based. In general, the bridge system is more stable against overturning compared with the frame system revealing a slightly different curve (i.e., higher sensitivity to medium-frequency pulses compared with low-frequency pulses in the corresponding frame system). However, a new shape of failure curve is integrated in the rocking response related to the abutment failure of the bridge structure, namely "sickle" shape. To this effect, the bridge is more prone to fail due to excessive longitudinal displacement induced by the deck to the abutment-backfill in the medium-to-high frequency range compared with the overturning behaviour of the frame system. Thus, the simple frame model fails to capture the abutment failure mode which can precede the overturning of piers and, therefore, the frame model can be more conservative in some cases than the model accounting for the abutment-backfill system. Finally, the studied bridges and frames were subjected to spectrum-compatible artificial ground motions. It was observed that the frame model is not sufficient to predict the rocking motion of bridges because it considerably overestimates their seismic response in terms of rocking amplitudes, duration of response-history and, as a result, number of impacts at the rocking interfaces. This is attributed to the influence of the abutment-backfill system in the rocking response of the bridge, by suppressing and attenuating rocking motion when the superstructure pounds on the abutments. However, the frame model fails to predict the safety margin against failure of the bridge structure, thus it overestimates the bridge safety in

a performance assessment context. Therefore, it is important to include the abutment-backfill system in a comprehensive performance assessment of rocking bridges. Overall, this paper confirmed the notable dynamic performance of rocking bridges and reiterated that pier rocking is an attractive option for seismic resistant bridges.

ORCID

Ioannis M. Thomaidis https://orcid.org/0000-0002-8049-5984
Andreas J. Kappos https://orcid.org/0000-0002-5566-5021
Alfredo Camara https://orcid.org/0000-0002-1675-2640

REFERENCES

1. Mander JB, Cheng CT. Seismic resistance of bridge piers based on damage avoidance design. *Technical Report*, *National Center for Earthquake Engineering Research*, State University of New York, Buffalo: New York, USA, 1997.
2. Sakai J, Mahin SA. Mitigation of residual displacements of circular reinforced concrete bridge columns. *Proceedings 13th World Conference on Earthquake Engineering*, *Vancouver*, *Canada*, 2004.
3. Makris N. A half-century of rocking isolation. *Earthq Struct*. 2014;7(6):1187-1221.
4. DeJong MJ. Amplification of rocking due to horizontal ground motion. *Earthq Spectra*. 2012;28(4):1405-1421.
5. Palermo A, Pampanin S, Calvi GM. Concept and development of hybrid solutions for seismic resistant bridge systems. *J Earthq Eng*. 2005;9(6):899-921.
6. ElGawady MA, Sha'Ian A. Seismic behavior of self-centering precast segmental bridge bents. *J Bridge Eng*. 2011;16(3):328-339.
7. Sideris P. Nonlinear quasi-static analysis of hybrid sliding-rocking bridge columns subjected to lateral loading. *Eng Struct*. 2015;101:125-137.
8. Hao H, Zhou Y. Rigid structure response analysis to seismic and blast induced ground motions. *Proced Eng*. 2011;14:946-955.
9. Ou Y, Chiewanichakorn M, Aref AJ, Lee GC. Seismic performance of segmental precast unbonded posttensioned concrete bridge columns. *J Struct Eng*. 2007;133(11):1636-1647.
10. ElGawady M, Booker AJ, Dawood HM. Seismic behavior of posttensioned concrete-filled fiber tubes. *J Compos Constr*. 2010;14(5):616-628.
11. Beck JL, Skinner RI. The seismic response of a reinforced concrete bridge pier designed to step. *Earthq Eng Struct Dyn*. 1974;2:343-358.
12. Ma QT, Khan MH. Free vibration tests of a scale model of the south Rangitikei railway bridge. *Proceedings New Zealand Society for Earthquake Engineering Conference*, 2008.
13. Chouw N. Low-damage design philosophy for future earthquake-resistant structures. Proceedings of the ASME Pressure Vessels and Piping Conference, Waikoloa, Hawaii, USA, 2017.
14. Routledge PJ, Cowan MJ, Palermo A. Low-damage detailing for bridges—a case study of Wigram-Magdala bridge. *Proceedings New Zealand Society for Earthquake Engineering Conference*, 2016.
15. Housner GW. The behavior of inverted pendulum structures during earthquakes. *Bull Seismol Soc Am*. 1963;53(2):403-417.
16. Zhang J, Makris N. Rocking response of free-standing blocks under cycloidal pulses. *J Eng Mech*. 2001;127(5):473-483.
17. DeJong MJ, Dimitrakopoulos EG. Dynamically equivalent rocking structures. *Earthq Eng Struct Dyn*. 2014;43:1543-1563.
18. Makris N, Vassiliou MF. Planar rocking response and stability analysis of an array of free-standing columns capped with a freely supported rigid beam. *Earthq Eng Struct Dyn*. 2013;42:431-449.
19. Dimitrakopoulos EG, Giouvanidis AI. Seismic response analysis of the planar rocking frame. *J Eng Mech*. 2015;141(7):04015003.
20. Aviram A, Mackie KR, Stojadinovic B. Effect of abutment modeling on the seismic response of bridge structures. *Earthq Eng Eng Vibr*. 2008;7(4):395-402.
21. Wilson P, Elgamal A. Full-scale bridge abutment passive earth pressure experiment and simulation. *ASCE J Geotech Geoenviron Eng*. 2010;136(12):1634-1643.
22. Shamsabadi A, Khalili-Tehrani P, Stewart JP, Taciroglou E. Validated simulation models for lateral response of bridge abutments with typical backfills. *J Bridge Eng*. 2010;15(3):302-311.
23. Xie Y, Huo Y, Zhang J. Development and validation of p-y modeling approach for seismic response predictions of highway bridges. *Earthq Eng Struct Dyn*. 2017;46:585-604.
24. Xie Y, Zheng Q, Yang C-SW, et al. Probabilistic models of abutment backfills for regional seismic assessment of highway bridges in California. *Eng Struct*. 2019;180:452-467.
25. Taskari O, Sextos A. Multi-angle, multi-damage fragility curves for seismic assessment of bridges. *Earthq Eng Struct Dyn*. 2015;44:2281-2301.
26. Agalianos A, Psychari A, Vassiliou MF, Stojadinovic B, Anastasopoulos I. Comparative assessment of two rocking isolation techniques for a motorway overpass bridge. *Front Built Environ*. 2017;3(47).
27. Roh H, Reinhorn AM. Modeling and seismic response of structures with concrete rocking columns and viscous dampers. *Eng Struct*. 2010;32:2096-2107.
28. Kappos AJ, Potikas P, Sextos AG. Seismic assessment of an overpass bridge accounting for non-linear material and soil response and varying boundary conditions. Proceedings of the ECCOMAS Thematic Conference on Computational Methods in Structural Dynamics and Earthquake Engineering, Rethymno, Crete, Greece, 2007.

29. Vassiliou MF. Seismic response of a wobbling 3D frame. *Earthq Eng Struct Dyn*. 2017;1-17.
30. Shenton HW. Criteria for initiation of slide, rock, and slide-rock rigid-body modes. *J Eng Mech*. 1996;122(7):693-693.
31. Taniguchi T. Non-linear response analyses of rectangular rigid bodies subjected to horizontal and vertical ground motion. *Earthq Eng Struct Dyn*. 2002;31:1481-1500.
32. Pompei A, Scalia A, Symbatyan MA. Dynamics of rigid block due to horizontal ground motion. *J Eng Mech*. 1998;124(7):713-171.
33. Makris N, Vassiliou MF. Are some top-heavy structures more stable? *J Struct Eng*. 2014;140(5):06014001.
34. Cheng C. Energy dissipation in rocking bridge piers under free vibration tests. *Earthq Eng Struct Dyn*. 2007;36:503-518.
35. Di Egidio A, Contento A. Base isolation of slide-rocking non-symmetric rigid blocks under impulsive and seismic excitations. *Eng Struct*. 2009;31:2723-2734.
36. Kalliontzis D, Sritharan S, Schultz A. Improved coefficient of restitution estimation for free rocking members. *J Struct Eng*. 2016;142(12): 06016002.
37. Jankowski R. Theoretical and experimental assessment of parameters for the non-linear viscoelastic model of structural pounding. *J Theoretic Appl Mech*. 2007;45(4):931-942.
38. Roh H, Reinhorn AM. Analytical modeling of rocking elements. *Eng Struct*. 2009;31:1179-1189.
39. ElGawady MA, Ma Q, Butterworth JW, Ingham J. Effects of interface material on the performance of free rocking blocks. *Earthq Eng Struct Dyn*. 2011;40:375-392.
40. Muthukumar S, DesRoches R. A hertz contact model with non-linear damping for pounding simulation. *Earthq Eng Struct Dyn*. 2006; 35:811-828.
41. Shi Z, Dimitrakopoulos EG. Comparative evaluation of two simulation approaches of deck-abutment pounding in bridges. *Eng Struct*. 2017;148:541-551.
42. Kwon O, Elnashai AS. Fragility analysis of a highway over-crossing bridge with consideration of soil-structure interactions. *Struct Infrastruct Eng*. 2010;6(1–2):159-178.
43. EN 1998–1. Eurocode 8: design of structures for earthquake resistance—part 1: general rules, seismic actions and rules for buildings, 2004.
44. Caltrans. Seismic design criteria version 2.0. State of California Department of Transportation, Sacramento, USA, 2019.
45. Mylonakis G, Nikolaou S, Gazetas G. Footings under seismic loading: analysis and design issues with emphasis on bridge foundations. *Soil Dyn Earthq Eng*. 2006;26:824-853.
46. Kirkpatrick P. Seismic measurements by the overthrow of columns. *Bull Seismol Soc Am*. 1927;17:95-109.
47. Dimitrakopoulos EG, DeJong MJ. Revisiting the rocking block: closed-form solutions and similarity laws. *Proc Royal Soc A*. 2012;468: 2294-2318.
48. Vassiliou MF, Makris N. Analysis of the rocking response of rigid blocks standing free on a seismically isolated base. *Earthq Eng Struct Dyn*. 2012;21:177-196.
49. MATLAB. version 9.1.0.441655 (R2016b). Natick, Massachusetts: The MathWorks Incorporation, 2016.
50. Papadrakakis M, Mouzakis H, Plevris N, Bitzarakis S. A Lagrange multiplier solution for pounding of buildings during earthquakes. *Earthq Eng Struct Dyn*. 1991;20:981-998.
51. Athanassiadou CJ, Penelis GG, Kappos AJ. Seismic response of adjacent buildings with similar or different dynamic characteristics. *Earthq Spectra*. 1994;10:293-317.
52. Malhotra PK. Dynamics of seismic pounding at expansion joints of concrete bridges. *J Eng Mech*. 1998;124:794-802.
53. Gkatzogias KI. Performance-based seismic design of concrete bridges for deformation control through advanced analysis tools and control devices. Doctor of Philosophy Thesis, City, University of London, London, UK, 2017.
54. Mathey C, Feau C, Politopoulos I, Clair D, Baillet L, Fogli M. Behavior of rigid blocks with geometrical defects under seismic motion: an experimental and numerical study. *Earthq Eng Struct Dyn*. 2016;45:2455-2474.

How to cite this article: Thomaidis IM, Kappos AJ, Camara A. Dynamics and seismic performance of rocking bridges accounting for the abutment-backfill contribution. *Earthquake Engng Struct Dyn*. 2020;49:1161–1179. https://doi.org/10.1002/eqe.3283